



Influence of Mechanical Alloying and Sintering Temperature on the Microstructure and Mechanical Properties of a Ti-22Al-25Nb Alloy

Wei Wang, Haixiong Zhou, Qingjuan Wang, Yuan Gao, and Kuaishe Wang

(Submitted June 20, 2019; in revised form January 11, 2020; published online February 6, 2020)

In this research, a fine-grained Ti-22Al-25Nb (at.%) alloy was fabricated from the powders of Ti, Al and Nb by mechanical alloying (MA) and subsequent spark plasma sintering (SPS). The effects of MA and SPS parameters on the microstructure, micro-hardness and tribological properties of the sintered compacts were investigated and discussed. The single phase of (Ti, Al, Nb) bcc solid solution with the chemical composition of Ti-22Al-25Nb was produced by MA for 5-20 h and the rotation speed of 500 rpm. The mechanically alloyed powders for 5, 10, 15 and 20 h were subsequently consolidated by SPS at the temperature range of 1000-1300 °C for 60 min, respectively, followed by furnace cooling. The microstructures from the sintered compacts showed that the fine equiaxed B2 phase, the lamellar or equiaxed O phase, and the equiaxed α_2 phase were present in all the sintered compacts. The highest micro-hardness value of 1840 HV_{0.3} and the smallest wear rate of 1.59×10^{-3} mm³/m were exhibited in the Ti-22Al-25Nb alloy sintered at 1100 °C/60 min/50 MPa.

Keywords Ti-22Al-25Nb alloy, mechanical alloying, mechanical properties, spark plasma sintering, tribological properties

1. Introduction

Since the discovery of orthorhombic (O) phase in 1988, Ti₂AlNb-based alloy (Ref 1) as a promising lightweight and high-temperature structural material has a wide application prospect in aerospace due to its advantages of low density, high strength and high creep resistance (Ref 2-4). In the past few years, numerous studies have been carried out on the casting, rolling, forging, plastic processing and heat treatment of the Ti₂AlNb-based alloy (Ref 5-8). The main purpose of these researches was set on the elimination of disadvantages such as microstructure segregation and inhomogeneity (Ref 9, 10). That is because the density and diffusion coefficient of Ti, Al and Nb elements are much different. In recent years, powder metallurgy (PM) method has been applied to the fabrication of the Ti₂AlNb-based alloy. This technique could resolve the segregation of microstructure and inhomogeneity of chemical composition and obtain an ultrafine microstructure.

Currently, there are several PM methods to fabricate the Ti₂AlNb-based alloy like vacuum hot pressing (HP) of Ti₂AlNb pre-alloyed powder (Ref 11) and the powders of Ti, Al and Nb (Ref 12, 13), and hot isostatic pressing (HIP) of pre-alloyed powders (Ref 14, 15). However, these PM methods result in many disadvantages such as voids and coarse grain size produced by long sintering time. In order to eliminate these shortcomings, the spark plasma sintering (SPS) technique has been applied to the fabrication of Ti₂AlNb-based alloys. This technique helps to achieve fine and homogeneous microstructure (Ref 4, 5). In SPS, the plasma activated by a pulsed current could realize the rapid consolidation of powders at a low sintering temperature. Owing to the essential characteristics of SPS, when this technique is combined with mechanical alloying (MA), the homogeneous microstructure with fine or ultrafine grain size could be obtained. Mechanical alloying is a complex physical and chemical processes that lead to repeated deformation, cold welding and crushing of the powders by high-energy ball milling, and finally achieve atomic-level alloying between elements (Ref 16, 17). Some endeavors have been devoted to obtain Ti₂AlNb-based alloy powders by MA from the powders of Ti, Al and Nb, and as a result, the powders with uniform and ultrafine particles were fabricated by MA in a high-energy planetary ball mill (Ref 18, 19). The time of mechanical alloying and the temperature of sintering play important roles in the final microstructures and mechanical properties of the material (Ref 18-20). However, there are few reports on this aspect in the current research.

In this paper, the Ti₂AlNb alloy was produced by MA and SPS technique with the powders of Ti, Al and Nb as the initial materials. The effects of MA parameters on the morphology and phase composition of the mechanically alloyed powder were investigated. The effects of the SPS parameters on the microstructure and mechanical properties of the sintered compacts were also investigated. In addition, the changes in micro-hardness and tribological properties were evaluated.

Wei Wang, Haixiong Zhou, Qingjuan Wang, Yuan Gao, and Kuaishe Wang, School of Metallurgy Engineering, Xi'an University of Architecture and Technology, Xi'an 710055, China. Contact e-mails: gackmol@163.com and jian dawqj@163.com.

2. Materials and Experimental Methods

In this experiment, Ti-22Al-25Nb alloy was fabricated by powder metallurgy method. The schematic diagram of the preparation methods on Ti-22Al-25Nb is shown in Fig. 1. The mechanical alloying and spark plasma sintering were used in this preparation process. The powders of Ti (purity > 99.9%, particle < 300 mesh), Al (purity > 99.9%, particle < 500 mesh) and Nb (purity > 99.9%, particle < 300 mesh) were used as starting materials. The Ti, Al and Nb powders were blended in the atomic ratio of 53:22: 25 using an argon-protected V-type mixer for 2 h.

The mixed powders were put into a stainless steel vial with the stainless steel balls. The diameters of the stainless steel balls are 10 and 5 mm, respectively. The weight ratio of the large ball to the small ball was 1:5. In order to avoid the oxidation of the mixed powders, the argon gas was added to the stainless steel vial before ball milling. The weight ratio of the mixed powder to the ball was 1:10. The rotation speed is 300 r/min. And then, the stainless steel vial was added to the QM-3SP2 planetary ball mill to study the effects of the mechanical alloying parameters on the deformation morphology and chemical composition of the mixed powders. In order to evaluate the effect of milling time on the microstructure, different milling times of 5, 10, 15 and 20 h were set. The mixed powders after ball milling were put into a high-strength graphite mold, and then sintered at four different temperatures of 1000, 1100, 1200 and 1300 °C. During sintering, the heating rate, pressure and the holding time were 100 °C/min, 50 MPa and 60 min.

The morphology and microstructure of the mechanically alloyed powders and spark plasma-sintered (SPSed) Ti-22Al-25Nb alloys were analyzed with an x-ray diffractometer (XRD) and a scanning electron microscope (SEM). The phase transformation characteristics were characterized by Netzsch thermo-gravimetry differential scanning calorimetry (TG-DSC) by heating mechanically alloyed Ti-22Al-25Nb powders from room temperature to 1400 °C at a rate of 10 °C/min. Subsequently, the micro-hardness of the compacts was evaluated using an HVS-1000 Z-type digital micro-hardness tester with an experimental load of 300 g and a holding time of 10 s. Each specimen was measured at least five indentations to obtain the average results. The tribological tests were performed on the BRUKER UMT-3 ball on disk reciprocating friction and wear tester at ambient conditions. The upper sample is the GCr15

bearing steel (a diameter of 3 mm, hardness about HRC 58 and surface roughness about 0.01 μm). The lower sample is the prepared samples with the dimensions of 20 mm (diameter) × 3 mm. In the tribological test, the applied load was 3 N, and the frequency and the linear speed was 15 Hz and 0.03 m/s, respectively. The coefficient of friction (COF) was automatically and continuously recorded. The wear scars on the ball and disk were measured with a Micro-XAM-3D surface profiler. The wear volume of the ball side is follows:

$$V = \left(\frac{\pi l}{6}\right) \left(\frac{3d^2}{4} + l^2\right) \quad (\text{Eq 1})$$

$$l = r - \sqrt{r^2 - \frac{d^2}{4}} \quad (\text{Eq 2})$$

where V is the wear volume, r is the radius of the ball, d is the wear scar diameter and l is the worn height of the ball.

3. Results and Discussion

3.1 Morphology and Microstructure of Mechanically Alloyed Powder

Figure 2 shows the SEM and XRD images of the mixed powders in a V-type mixer for 2 h. From the SEM image (Fig. 2a), the surface of Al powder particles is smooth and the Ti and Nb powder particles are irregular. From the XRD results (Fig. 2b), it can be seen that the peaks of Ti, Al and Nb elements were observed as the main phases. This indicates that no reaction and interdiffusion occurred among Ti, Al and Nb elements in the mixed powders. From the XRD patterns of the mechanical alloyed powders for different times (Fig. 3), it can be seen that as the ball milling time increased, the intensity and broadness of the diffraction peaks of Ti, Al and Nb were decreased. Due to lattice distortion and grain boundary fragmentation of the powder particles during ball milling, the changes in peak intensity indicate that the diffusion was occurred among the Ti, Al and Nb elements. After ball milling for 5 h, the Ti₂AlNb peak appeared at 2θ = 37.2, and the Al peak at 2θ = 44.7 and 78.2 disappeared substantially. In the mechanical alloying, the solid solutions of (Ti, Al) and (Al, Nb) were formed. The reason is that the most of the Al dissolved into the crystal lattice of Ti and Nb by mutual penetration

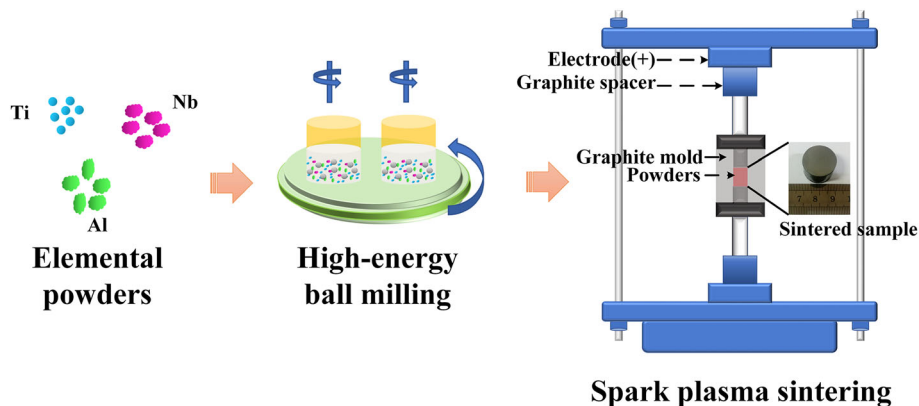


Fig. 1 Schematic illustration of procedures to fabricate Ti-22Al-25Nb alloy

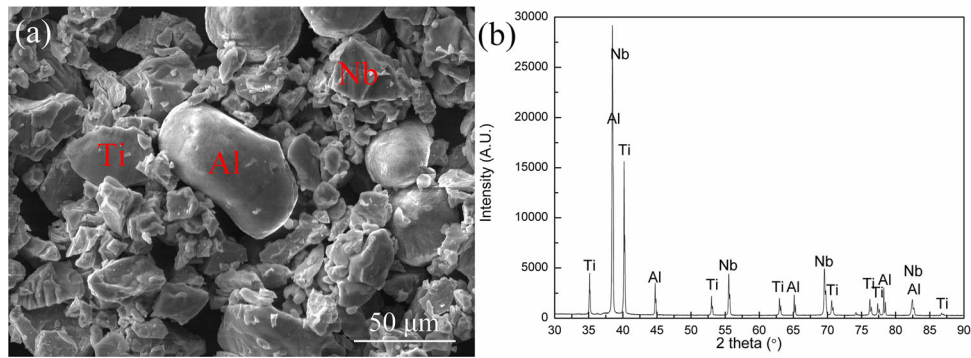


Fig. 2 Ti-22Al-25Nb powder mixed in a V-type mixer (a) SEM image; (b) XRD pattern

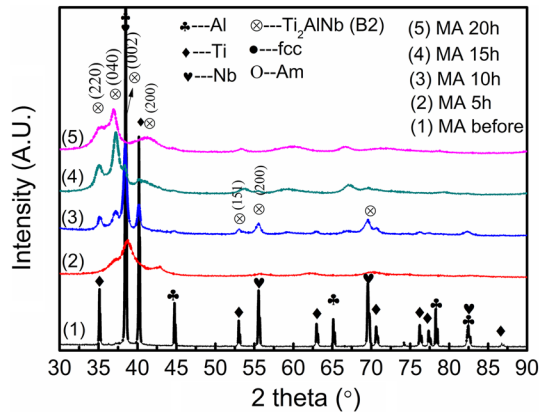


Fig. 3 XRD patterns of the mixed powder after mechanical alloying for 5, 10, 15 and 20 h at a rotation speed of 300 rpm

gradually. The diffraction peaks of Ti, Al and Nb at $2\theta = 38.4$ after ball milling for 15 h disappeared completely. The diffraction peak of Nb elements at 2θ of 55.5 and 69.5 disappeared, and the residual Nb merged with the lattice of (Ti, Al) solid solution. As the ball milling time increased to 15 h, the diffraction peaks of Ti at $2\theta = 35.1, 40.1$ and 53 disappeared completely. At the same time, only the Ti_2AlNb diffraction peaks with low intensity and wider width appeared. Finally, the residual Ti also merged into the lattice of (Al, Nb) solid solution. And then, the homogeneous solid solution was formed. It is illustrated that after ball milling for 20 h, a solid solution with the body-centered cubic structure can be formed by interdiffusion of Ti, Al and Nb elements.

The SEM and elemental distribution image of the mechanical alloyed powders are shown in Fig. 4. It can be observed that after mechanical alloying for 5 h (Fig. 4a), the powders are unevenly distributed. The shape of the powders is irregular. As the time of mechanical alloying increased, the powder particles were gradually transformed into a spherical shape (Fig. 4(e) and (i)). After mechanical alloying for 15 h (Fig. 4i and m), the powder particles became fine spheres. Its grain size can reach the nanocrystalline level. As the mechanical alloying time increased, the size of the powders decreased. And the distribution of elements becomes more uniform. In the process of mechanical alloying, the powders are crushed over and over, and finally welded. As the time of mechanical alloying was increased to 20 h, the mixed powders became finer. The particle size of the mixed powders is about 2 μm due to aggregation in the powders.

Figure 5 illustrates DTA curve of the mixed powders after ball milling for 5, 10, 15 and 20 h, respectively. It can be observed that there are no decalescence peaks of Al element near the temperature of 660 $^{\circ}\text{C}$ (the melting point of Al). However, when the temperature was below 660 $^{\circ}\text{C}$, an exothermic peak appeared. It means that the element Al has completely reacted with the element Ti, and formed a new phase, TiAl. The mixed powders formed a large amount of metal compound. And at the same time, the weight loss also reached the maximum at this temperature. After the ball milling for 15 h, the grain size became smaller and reached the nanocrystalline level. Due to the smaller particle size, the reaction energy was reduced. So the exothermic peak was formed. After the ball milling for 20 h, the temperature of the exothermic peak is lower due to the low stability of the amorphous phase. In conclusion, from Fig. 6, at the initial stage, the powders of Al, Ti and Nb were blended. And then, as the MA time increased to 5 h, the amounts of Ti and Al decreased, most of the Al was dissolved into Ti and Nb lattices to form (Al, Ti) and (Nb, Al) solid solution by interpenetration. During MA, the powders exceed the limitation of the equilibrium solid solubility. The metastable supersaturated solid solutions by MA were formed. Thus, as the MA time increased to 15 h, the residual Ti and (Al, Nb), and the residual Nb and (Al, Ti) solid solutions merged and formed the (Ti, Al, Nb) solid solutions. However, in the MA powders, the residual Nb powders also existed. Finally, the (Ti, Al, Nb) solid solutions formed completely.

3.2 Phase Composition and Microstructural Evolution of Spark Plasma-Sintered Compacts

Figure 7 shows the XRD patterns of SPS sintered samples at 1000, 1100, 1200 and 1300 $^{\circ}\text{C}$. It can be observed that B2 phase was the main phase in the sample sintered at 1000 $^{\circ}\text{C}$ after the ball milling for 5 h. Only a little of O and α_2 phases were found in this microstructure. The diffraction peak of the O phase gradually increased as the temperature increased. The main phase of B2 and O and a small amount of α_2 phase occurred in the microstructure of the samples sintered by SPS at 1300 $^{\circ}\text{C}$. As the sintering temperature increased, the intensity of the O phase diffraction peak increased. When the sintering temperature increased to 1300 $^{\circ}\text{C}$, the O phase was the main phase, accompanied by a small amount of the B2 and α_2 phases. No matter how long the time of ball milling (5 or 20 h), the intensity of the O phase diffraction peak gradually increased with the increase in the sintering temperature. However, it can be found that more diffraction peaks of the O phase were

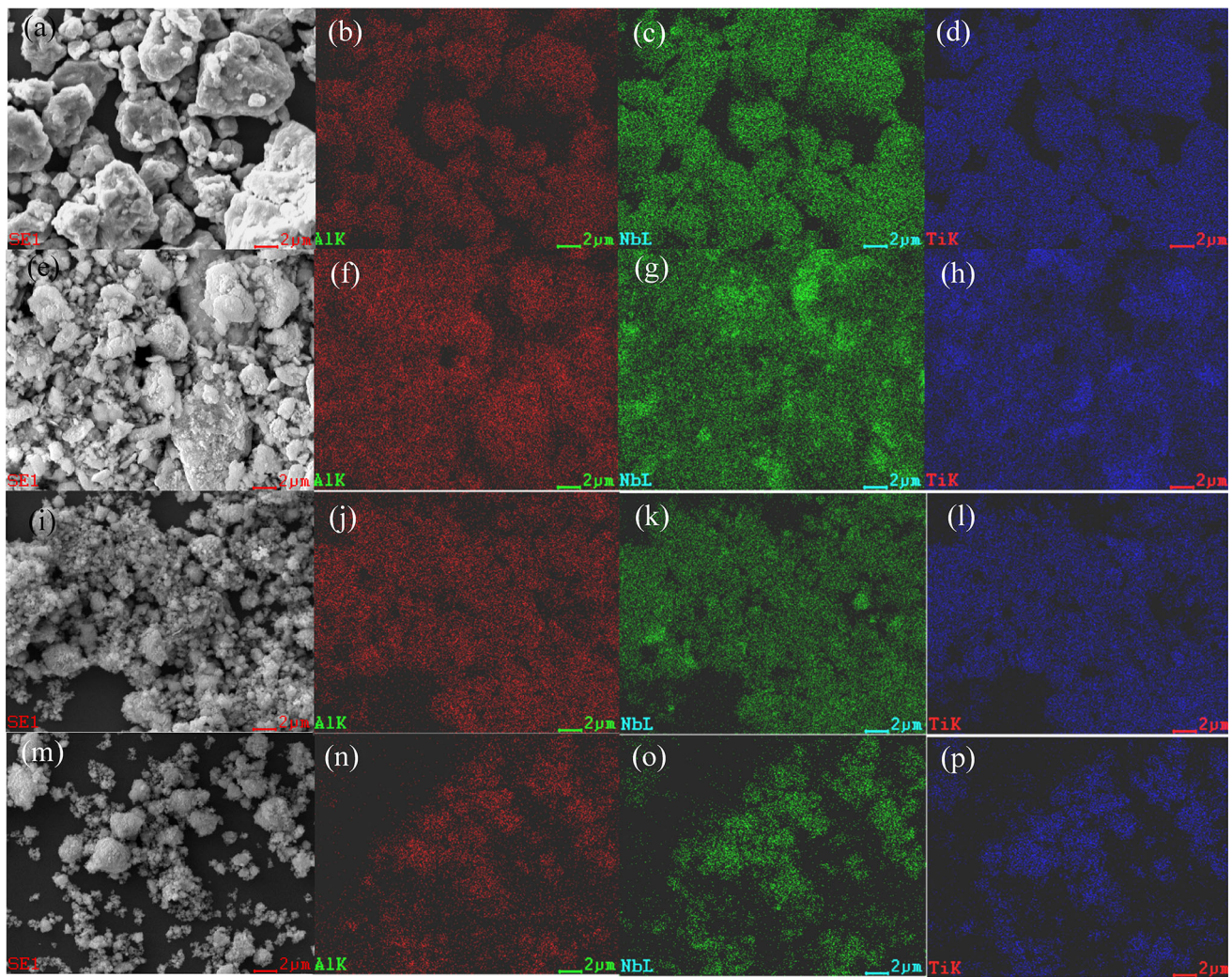


Fig. 4 SEM and elemental distribution of Ti-22Al-25Nb powder after different ball milling times (a-d) MA5 h (e-h) MA10h, (i-l) MA15h, (m-p) MA20 h

formed and a little of the diffraction peaks of B2 and α_2 phase were formed at the same sintering temperature. And the diffraction peak of O phase is more obvious at lower sintering temperature. Therefore, it is very beneficial to increase the time of ball milling and the sintering temperature. It can promote the reaction between Ti, Al and Nb and form the new lamellar O phase.

Figures 8, 9, 10, and 11 show SEM images of samples subjected to different sintering temperatures and ball milling times. Figure 8 shows the SEM images of the sintered samples at 1000, 1100, 1200 and 1300 °C after ball milling for 5 h. The corresponding EDS analysis data are displayed in Table 1. It can be seen that the white, black and gray are B2 phase, α_2 phase and O phase, respectively. The distribution of the microstructure was very uneven at 1000 °C, and the major parts are B2 phases. As the sintering temperature increases, the uniformity of the microstructure increased, and the volume fraction of O phase also increased gradually. As the sintering temperature increased to 1300 °C, the gray O phase and the white B2 phase region were considered as main portions. It is similar to the XRD analysis of Fig. 7(a). It was also found that the increase in the sintering temperature can promote the diffusion of alloying elements. As the sintering temperature

increased, the growth rate of the crystal grains also accelerated. So the crystal grains of the material are coarsened, and the mechanical properties of the material deteriorate. From Fig. 8, it is obvious that as the sintering temperature increases, the grain size of the material is gradually increased.

Figures 9, 10, and 11 show the SEM image of the samples prepared by sintering at 1000, 1100, 1200, and 1300 °C with MA10 h, MA15 h and MA20 h. The corresponding EDS analysis are displayed in Tables 2, 3 and 4. The variation tendencies are very similar to those shown in Fig. 8. As the sintering temperature increased, the uniformity of the microstructure also increased. And the size of the crystal grains became coarser. At same sintering temperature, as the ball milling time increases, the uniformity of the microstructure increases, the area of the O phase becomes larger, and the grain size becomes smaller. From Fig. 8, 9, 10 and 11, it can be observed that the microstructure of the sample is relatively uniform after ball milling for 5 h at the sintering temperature of 1200 °C. The distribution of the microstructure is uniform at the sintering temperature of 1000 °C after ball milling for 20 h. The longer the ball milling time, the better the uniformity of the obtained powder particles. So the microstructure of the sintered sample can be evenly distributed at a lower temperature. It can

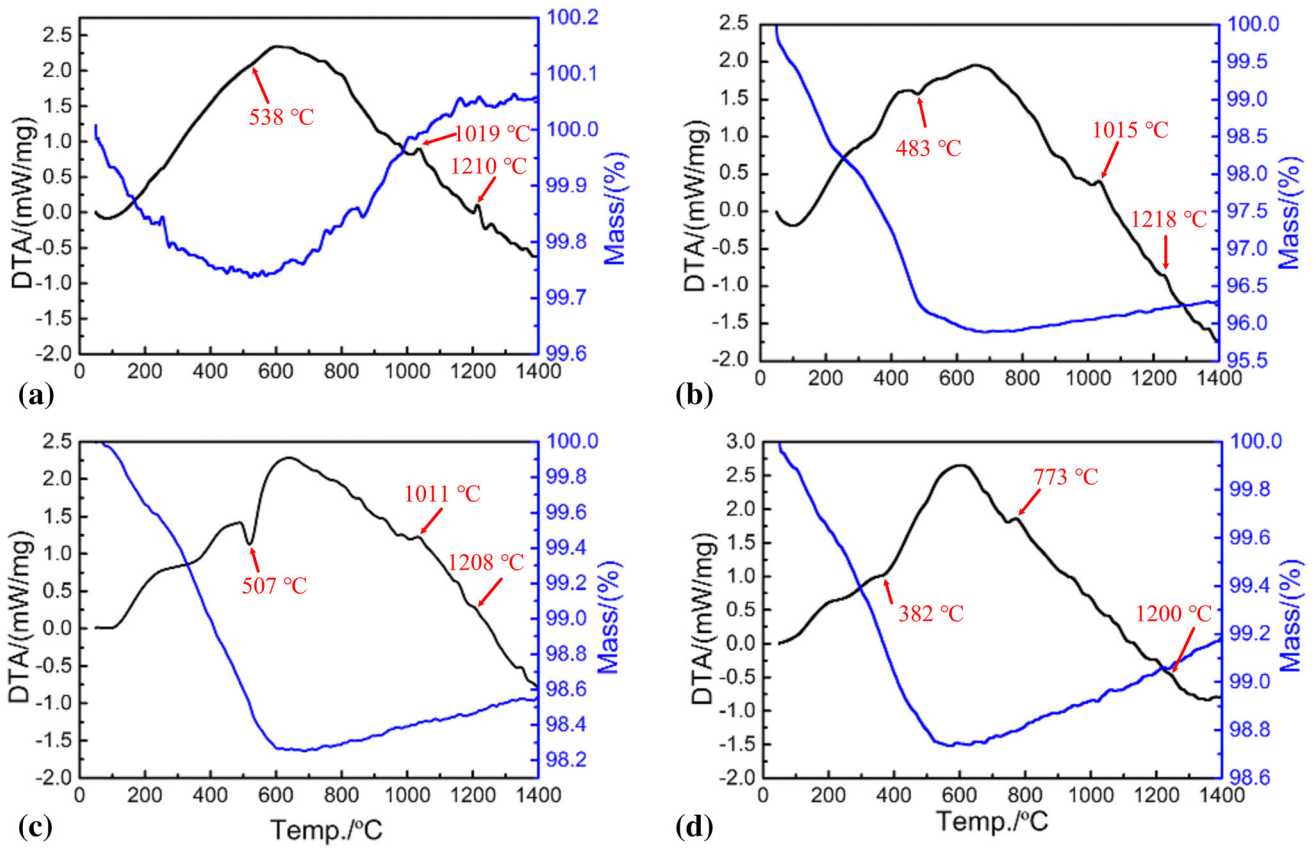


Fig. 5 DTA curve of Ti-22Al-25Nb powder after different ball milling times (a) MA5h, (b) MA10h, (c) MA15h and (d) MA20h

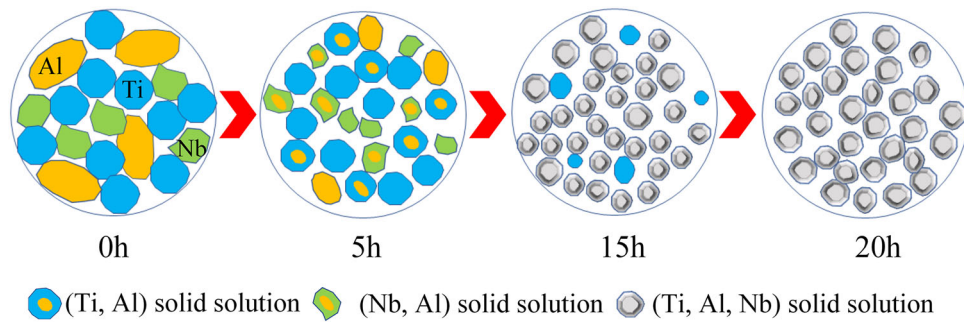


Fig. 6 Schematic illustration of the formation process of (Ti, Al, Nb) bcc solid solution during MA

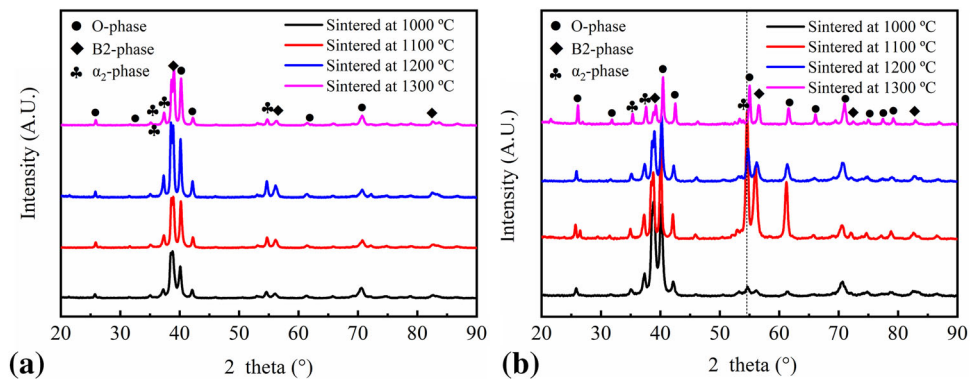


Fig. 7 XRD curve of Ti-22Al-25Nb alloy prepared at different sintering temperatures (a) MA5h; (b) MA20h

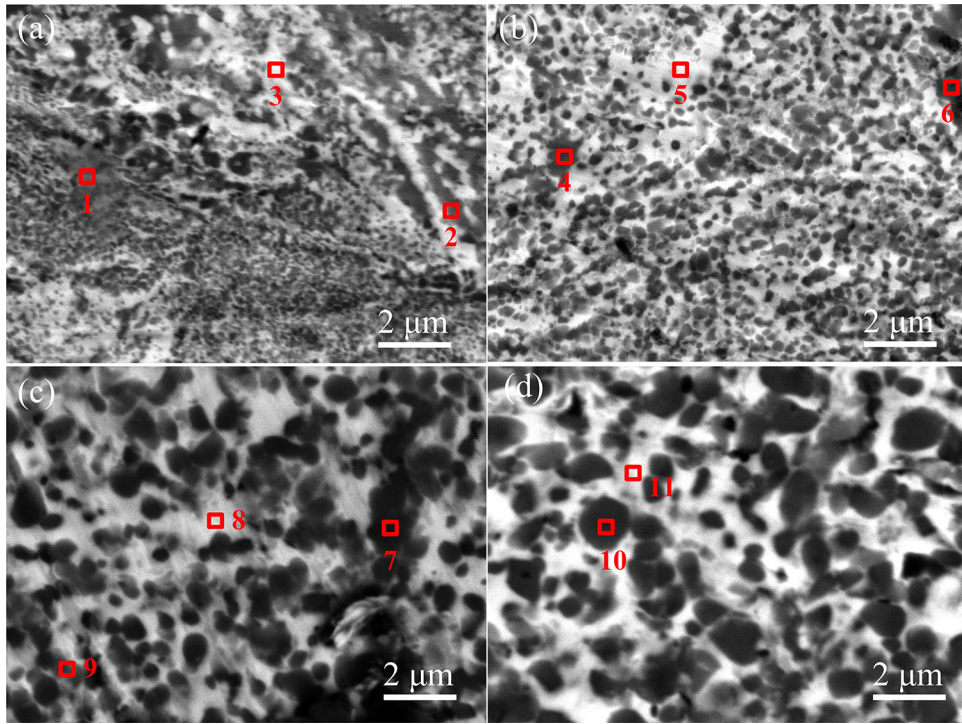


Fig. 8 SEM image of the samples prepared by SPS at different sintering temperatures after ball milling for 5 h, (a) = 1000, (b) = 1100, (c) = 1200 and (d) = 1300 °C

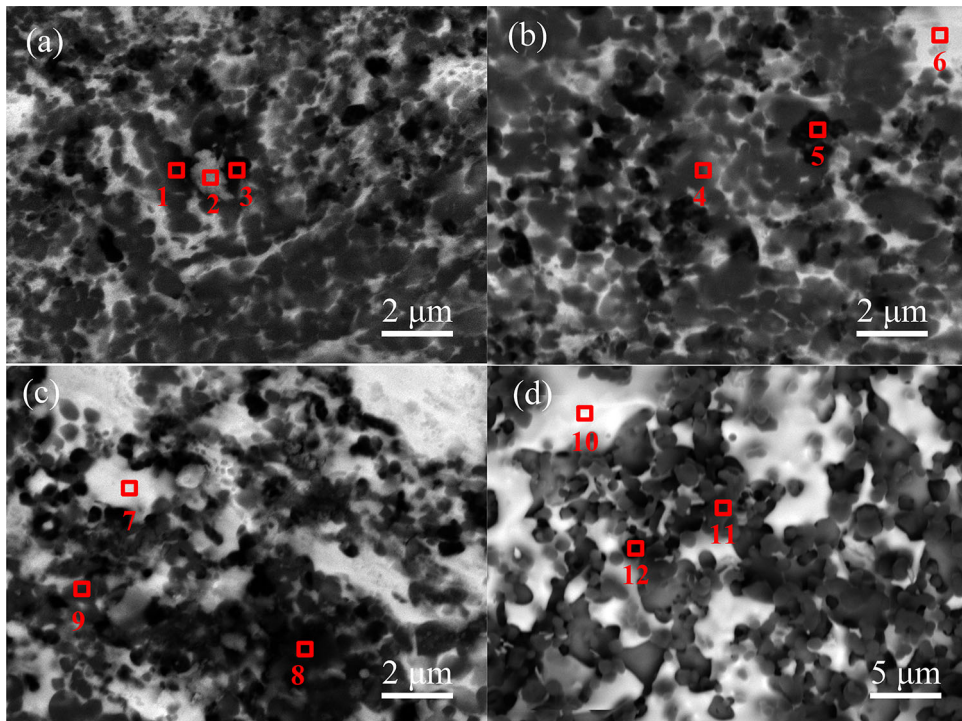


Fig. 9 SEM image of the samples prepared by SPS at different sintering temperatures after ball milling for 10 h

be observed in Fig. 7 that as the ball milling time increases, the diffraction peak of the O phase increases. It means that the volume fraction of O phase in the microstructure increases, and it can be clearly observed from Fig. 8, 9, 10 and 11.

Figure 12(a) and (b) depict TEM micrographs of the sample prepared by sintering at 1100 °C with ball milling for 20 h. TEM micrographs reveal the subtle morphology of α_2 and O phase precipitated from the B2 grain boundary and interior,

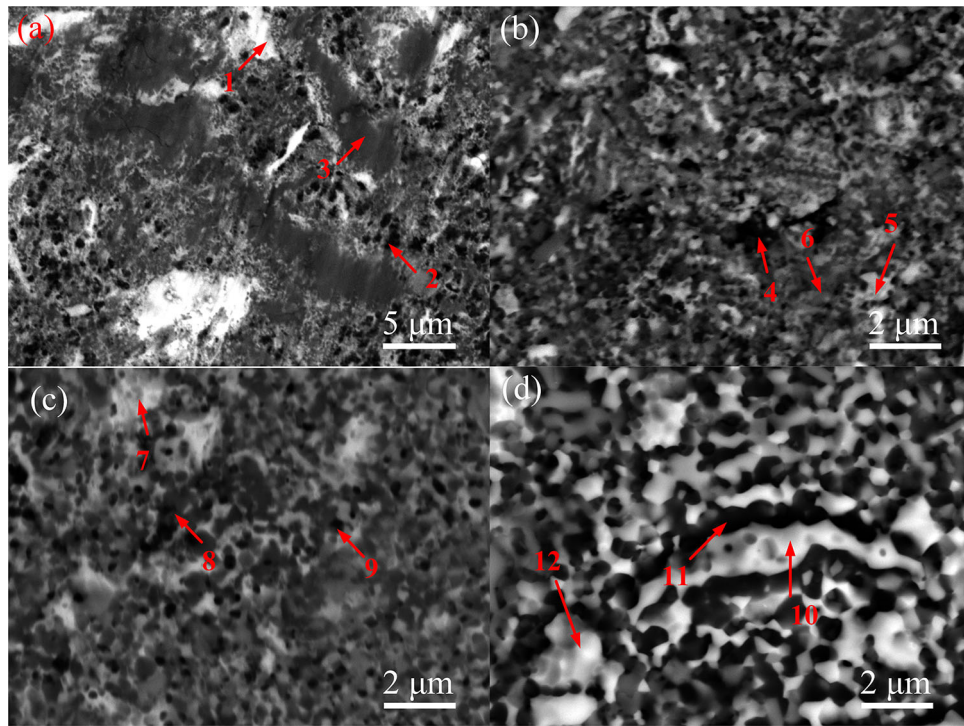


Fig. 10 SEM image of the samples prepared by SPS at different sintering temperatures after ball milling for 15 h

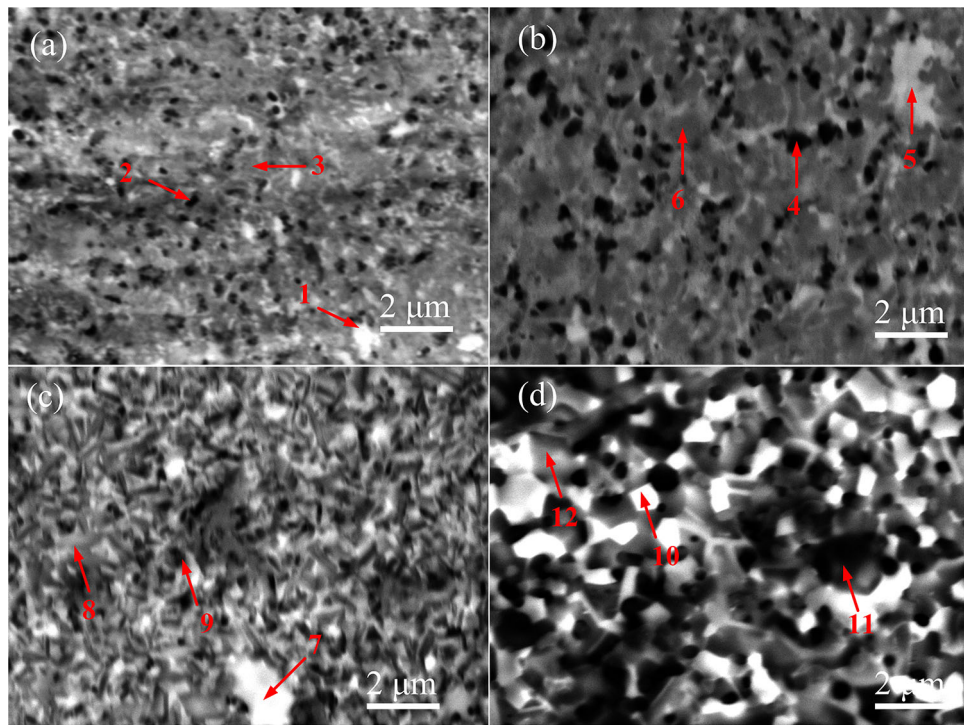


Fig. 11 SEM image of the samples prepared by SPS at different sintering temperatures after ball milling for 20 h, (a) = 1000, (b) = 1100, (c) = 1200 and (d) = 1300 °C

respectively. The acicular O phases are precipitated in the B2 grain interior, and the equiaxed α_2 -phases are distributed along the B2 grain boundary. The precipitation of acicular O phases is mainly attributed to the rapid cooling speed and short SPS time.

3.3 Micro-Hardness and Tribological Properties of Spark Plasma-Sintered Specimens

Figure 13 shows the micro-hardness variations of the samples at different ball milling times and sintering tempera-

Table 1 The EDS analysis (at.%) for different positions at ball milling for 5 h

Position	Phase	Ti	Al	Nb
1	α_2	66.99	26.78	6.23
2	O	51.03	25.64	23.33
3	B2	46.77	24.37	28.86
4	O	49.83	23.78	26.39
5	B2	46.57	25.25	28.18
6	α_2	65.23	27.52	7.25
7	α_2	67.82	26.13	5.87
8	B2	31.93	32.22	35.85
9	O	52.05	19.62	22.02
10	O	49.52	25.36	25.12
11	B2	42.01	27.19	30.80
12	α_2	69.32	25.76	4.92

Table 2 The EDS analysis (at.%) for different positions at ball milling for 10 h

Position	Phase	Ti	Al	Nb
1	B2	35.34	31.23	33.43
2	O	50.10	26.35	23.55
3	α_2	54.58	35.19	10.23
4	O	49.31	23.01	27.68
5	α_2	51.27	41.51	7.22
6	B2	32.28	29.44	38.27
7	B2	26.44	31.09	42.46
8	α_2	66.32	25.08	8.6
9	O	48.05	26.92	25.03
10	B2	19.71	36.95	43.34
11	O	49.68	27.60	22.72
12	α_2	66.99	26.78	6.23

Table 3 The EDS analysis (at.%) for different positions at ball milling for 15 h

Position	Phase	Ti	Al	Nb
1	B2	21.46	27.73	50.80
2	α_2	70.12	23.04	6.84
3	O	55.46	23.07	21.47
4	α_2	71.26	21.47	7.27
5	B2	37.04	31.47	31.50
6	O	51.79	25.75	22.45
7	B2	41.23	29.32	29.45
8	O	43.25	33.13	23.62
9	α_2	69.21	22.35	8.44
10	B2	29.77	29.95	40.27
11	α_2	68.96	21.87	9.17
12	O	43.10	29.50	27.40

tures. The results show that the micro-hardness of the compacts increases with the ball milling time. And at the same milling time, the micro-hardness first increased and then decreased with the increase in sintering temperature. When the sintering

Table 4 The EDS analysis (at.%) for different positions at ball milling for 20 h

Position	Phase	Ti	Al	Nb
1	B2	32.68	28.57	38.75
2	α_2	65.56	29.89	4.55
3	O	49.80	24.00	26.20
4	α_2	63.84	26.53	9.63
5	B2	44.00	25.32	30.69
6	O	55.04	19.55	25.41
7	B2	29.38	32.69	37.93
8	O	51.36	25.16	23.49
9	α_2	68.23	28.02	3.75
10	α_2	70.12	25.36	4.52
11	O	45.72	27.01	27.27
12	B2	20.64	39.88	39.48

temperature of the sample with ball milling for 20 h was increased from 1000 to 1100 °C, the micro-hardness increased from 1360 to 1840 HV. When the sintering temperature was greater than 1100 °C, the micro-hardness was decreased slightly. From Fig. 4, it can be seen that as the ball milling time increased, the particle size of the mixed powders after ball milling became smaller. The more uniform distribution was presented in the mixed powders. In the subsequent SPS, as observed in Fig. 8, 9, 10, and 11, with the increase in ball milling time, the uniformity of the microstructure was improved, and the grain size was reduced at the same sintering temperature. So, the increase in the ball milling time can refine powder particles and improve their uniformity. Thus, the decrease in the grain size of the sintered samples can improve the uniformity of microstructure and the micro-hardness of the sintered samples. It is also observed from Fig. 8, 9, 10 and 11 that with the increase in sintering temperature for the same ball milling time, the uniformity of the microstructure and the content of the O phase in the microstructure increased. However, the higher temperature will also increase the grain size, and the coarser grain size will reduce the mechanical properties of the material. Therefore, the micro-hardness of the sintered sample was firstly increased and then decreased.

Subsequently, the friction test was carried out on the samples sintered at different temperatures after ball milling for 20 h. The variation of the coefficient of friction (COF) with temperature is shown in Fig. 14. It can be seen that the initial COF increases with the increase in sintering temperature. The COFs at 1200 and 1300 °C are in the upward trend in the first 200 s, then enters the stable stage, and the values of COF remain around 0.45. Different sintering temperatures have almost no effect on COF after stabilization, but the fluctuations of the COF were reduced. The main reason why different sintering temperatures reduce the fluctuations of COF is that the microstructure uniformity of sintered materials increases with the increase in sintering temperature.

Figure 15 shows the wear rate of the sintered samples at different temperatures after ball milling for 20 h. The wear rate was firstly decreased and then increased with the increase in sintering temperature. The change trend of the COF was exactly opposite to the micro-hardness of the sintered sample after ball milling for 20 h. When the sintering temperature was increased to 1100 °C, the hardness value was the highest, and the corresponding wear rate was the lowest.

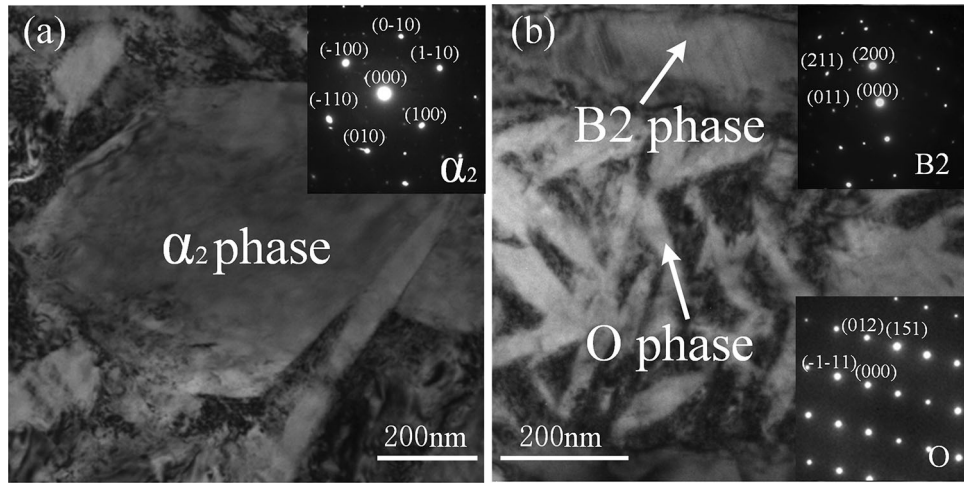


Fig. 12 (a), (b) TEM images and SAED pattern of the samples prepared by SPS at 1100 °C temperatures after ball milling for 20 h

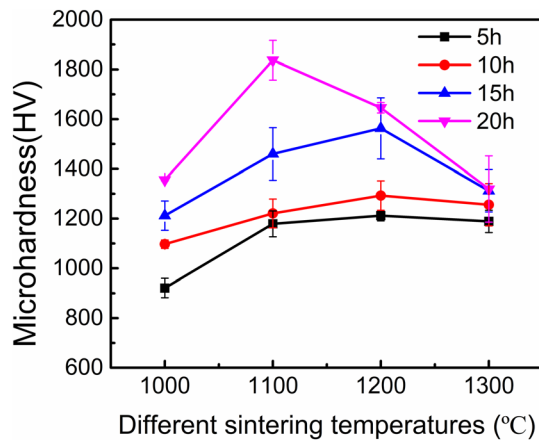


Fig. 13 Micro-hardness curves of Ti-22Al-25Nb alloy prepared at different ball milling times and different sintering temperatures

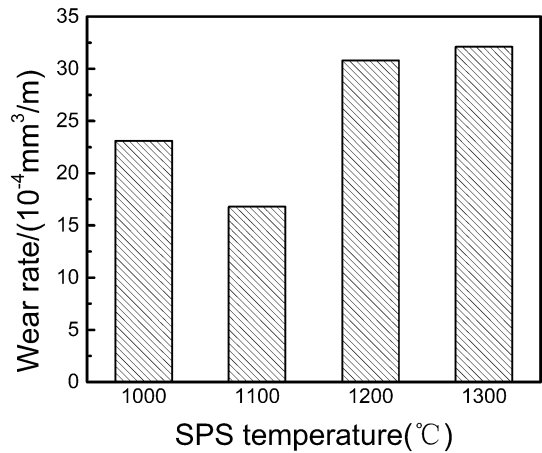


Fig. 15 Wear rate of Ti-22Al-25Nb alloy prepared by ball milling after 20 h at different sintering temperatures

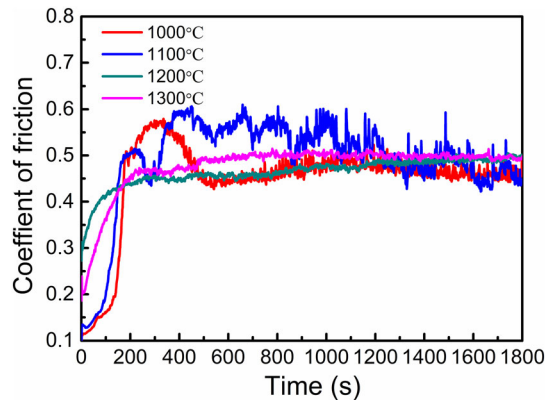


Fig. 14 Friction coefficient diagram of Ti-22Al-25Nb alloy prepared by ball milling after 20 h at different sintering temperatures

4. Conclusion

1. The Ti-22Al-25Nb alloy with uniform microstructure and fine grain size was successfully prepared by mechanical

alloying and spark plasma sintering using elemental powder.

- As the ball milling time increased, the size of the powder particles decreased. And a (Ti, Al, Nb) bcc solid solution having nanocrystals can be obtained by ball milling at 300 r/min for 20 h.
- After ball milling for 20 h, the alloy consisting of typical α_2 , O and B2 phases can be prepared by sintering at the sintering temperature of 1100 °C and the pressure of 50 MPa for 60 min.
- As the ball milling time increased, the micro-hardness of the alloy also increased. And as the sintering temperature increased, the micro-hardness first increased and then decreased. After ball milling for 20 h, the micro-hardness of the material was 1840 HV_{0.3} at a sintering temperature of 1100 °C.
- The effect of the sintering temperature is not obvious on the friction coefficient of the sample. The wear rate first decreased and then increased with the increase in the sintering temperature. When the sintering temperature is 1100 °C, the wear rate is the lowest.

Author Contributions

W.W., W. K. and Q. W. conceived and designed the experiments; W.W., Q. W. and H. Z. performed the experiments and analyzed the data; W.W. wrote the paper.

Funding

This work was supported by the fund of the National Natural Science Foundation of China (Nos. 51975450, 51605249), International Scientific and Technological Cooperation Program of the Shaanxi Province (Grant No. 2019KW-026), Basic Project of Education Department of Shaanxi Province (Grant No. 19JK0458) and the Tribology Science Fund of State Key Laboratory of Tribology (Grant No. SKLTKF18B02).

Conflicts of interest

The authors declare no conflict of interest.

References

1. W. Wang, W. Zeng, Y. Liu et al., Microstructural Evolution and Mechanical Properties of Ti-22Al-25Nb (at.%) Orthorhombic Alloy with Three Typical Microstructures[J], *J. Mater. Eng. Perform.*, 2018, **27**(1), p 293–303
2. S. Qu, S. Tang, A. Feng, C. Feng, J. Shen, and D. Chen, Microstructural Evolution and High-Temperature Oxidation Mechanisms of a Titanium Aluminide Based Alloy, *Acta Mater.*, 2018, **148**, p 300–310
3. W. Wang, W. Zeng, Y. Sun, H. Zhou, and X. Liang, Microstructure, Tensile, and Creep Behaviors of Ti-22Al-25Nb (at.%) Orthorhombic Alloy with Equiaxed Microstructure, *Materials*, 2018, **12**(4), p 1–13
4. Z. Wei, K. Hu, B. Sa, and B. Wu, Pressure-Induced Structure, Electronic, Thermodynamic and Mechanical Properties of Ti₂AlNb Orthorhombic Phase by First-Principles Calculations, *Rare Met.*, 2017, **11**, p 1–11
5. Y. Zheng, W. Zeng, D. Li, X. Liang, J. Zhang, and X. Ma, Effect of Orthorhombic Case on the Creep Rupture of Ti-22Al-25Nb (at.%) Orthorhombic Alloy, *Mater. Sci. Eng. A*, 2017, **696**, p 529–535
6. M. Li, Q. Cai, Y. Liu, Z. Ma, and Z. Wang, Microstructure and Mechanical Properties of Ti₂AlNb-Based Alloys Synthesized by Spark Plasma Sintering from Pre-Alloyed and Ball-Milled Powder, *Adv. Eng. Mater.*, 2017, **20**(4), p 17050659
7. Y. Zheng, W. Zeng, D. Li, Q. Zhao, X. Liang, and J. Zhang, Fracture Toughness of the Bimodal Size Lamellar α Phase Microstructures in

- Ti-22Al-25Nb (at.%) Orthorhombic Alloy, *J. Alloys Compd*, 2017, **709**, p 511–518
8. W. Wang, W. Zeng, C. Xue, X. Liang, and J. Zhang, Microstructure Control and Mechanical Properties from Isothermal Forging and Heat Treatment of Ti-22Al-25Nb (at.%) Orthorhombic Alloy, *Intermetallics*, 2015, **56**, p 79–86
 9. X. Liang, S. Li, J. Zhang, and Y. Cheng, Study of Hot Deformation Characteristics of an As-Cast Ti-22Al-25Nb Alloy, *Mater. Sci. Forum*, 2007, **546**, p 1461–1466
 10. A. Feng, B. Li, and J. Shen, Recent Advances on Ti₂AlNb-Based Alloys, *J. Mater. Metall.*, 2011, **9**, p 30–38
 11. J. Wu, R. Guo, L. Xu, Z. Lu, Y. Cui, and R. Yang, Effect of Hot Isostatic Pressing Loading Route on Microstructure and Mechanical Properties of Powder Metallurgy Ti₂AlNb Alloys, *J. Mater. Sci. Technol.*, 2017, **33**, p 172–178
 12. G. Wang, J. Yang, and X. Jiao, Microstructure and Mechanical Properties of Ti-22Al-25Nb Alloy Fabricated by Elemental Powder Metallurgy, *Mater. Sci. Eng. A*, 2016, **654**, p 69–76
 13. M. Li, Q. Cai, Y. Liu, Z. Ma, Z. Wang, and Y. Huang, Dual Structure O + B2 for Enhancement of Hardness in Furnace-Cooled Ti₂AlNb-Based Alloys by Powder Metallurgy, *Adv. Powder Technol.*, 2017, **28**, p 1719–1726
 14. H. Niu, Y. Chen, D. Zhang, Y. Zhang, J. Lu, and W. Zhang, Fabrication of a Powder Metallurgy Ti₂AlNb-Based Alloy by Spark Plasma Sintering and Associated Microstructure Optimization, *Mater. Des.*, 2016, **89**, p 823–829
 15. Z. Trzaska, A. Couret, and J. Monchoux, Spark Plasma Sintering Mechanisms at the Necks Between TiAl Powder Particles, *Acta Mater.*, 2016, **118**, p 100–108
 16. Z. Trzaska, G. Bonnefont, G. Fantozzi, and J.P. Monchoux, Comparison of Densification Kinetics of a TiAl Powder by Spark Plasma Sintering and Hot Pressing, *Acta Mater.*, 2017, **135**, p 1–13
 17. C. Suryanarayana, E. Ivanov, and V.V. Boldyrev, The Science and Technology of Mechanical Alloying, *Mater. Sci. Eng. A*, 2001, **304**, p 151–158
 18. K. Sim, G. Wang, R.C. Son, and S.L. Choe, Influence of Mechanical Alloying on the Microstructure and Mechanical Properties of Powder Metallurgy Ti₂AlNb-Based Alloy, *Powder Technol.*, 2017, **317**, p 133–141
 19. K. Sim, G. Wang, J. Jong-Min, J. Yang, and X. Li, Microstructure and Mechanical Properties of a Ti-22Al-25Nb Alloy Fabricated from Elemental Powders by Mechanical Alloying and Spark Plasma Sintering, *J. Alloys Compd*, 2017, **704**, p 425–433
 20. J. Wang, C. Wu, and Q. Shi, Preparation of Nanocrystalline Ti-6Al-4 V Alloy by Mechanical Alloying, *Rare Metal Mater Eng*, 2017, **46**, p 783–789

Publisher's Note Springer Nature remains neutral with regard to jurisdictional claims in published maps and institutional affiliations.